Molecular dynamics simulation of the orthobaric densities and surface tension of water

José Alejandre, Dominic J. Tildesley, and Gustavo A. Chapela

Additional information on J. Chem. Phys.

Molecular dynamics simulation of the orthobaric densities and surface tension of water

José Alejandre[a)] and Dominic J. Tildesley
Department of Chemistry, The University, Southampton SO9 5NH, United Kingdom

Gustavo A. Chapela
Departamento de Física, Universidad Autónoma Metropolitana-Iztapalapa, Apdo. Postal 55-534, 09340 México D.F, Mexico

Molecular dynamics simulations have been performed to study the liquid–vapor equilibrium of water as a function of temperature. The orthobaric densities and the surface tension of water are reported for temperatures from 316 K until 573 K. The extended simple point charge (SPC/E) interaction potential for water molecules is used with full Ewald summation. The normal and tangential components of the pressure tensor were calculated and are presented at 328 K. The nature of the long-range contribution to the surface tension has been studied in detail. At 328 K the calculated surface tension is 66.0 ± 3.0 mN m^{-1} in comparison with the experimental value of 67 mN m^{-1}. The simulated surface tensions between 316 K and 573 K are in good agreement with experiment. The orthobaric densities are in better agreement with experimental values than those obtained from the Gibbs ensemble calculation for the SPC model of water. © *1995 American Institute of Physics.*

I. INTRODUCTION

A knowledge of the liquid–vapor equilibrium in molecular systems is of considerable technological and academic importance. The search for straightforward and accurate simulation methods to study phase equilibria and the development of the corresponding potential models is an area of active research.[1–7]

There are a number of different approaches that can be used in the calculation of coexisting liquid and vapor densities by molecular simulation. The Gibbs simulation technique is a Monte Carlo method[8,9] (GEMC) which uses two boxes, one in each of the coexisting phases. Molecules are moved independently in each box and there are joint moves involving volume changes in both boxes and the exchange of molecules between the boxes. The method has been widely used to study phase equilibria of molecular systems.[5,10,11] The perceived advantage of the technique is the speed with which the coexisting phases are established from a starting configuration in the two-phase region. The principal disadvantage of the method is that molecule insertions can be difficult at the high densities close to triple point and that a number of sampling tricks such as rotational-bias[11] and the grid mapping of free insertion space[12] have to be used in this case. The Gibbs technique is not designed to study interfacial properties such as the surface tension. The method has been thoroughly reviewed by Smit.[7]

Phase boundaries can also be simulated by calculating the chemical potential and pressure as a function of density in the two coexisting phases and solving the Gibbs equations for the phase line. In particular the chemical potential can be calculated by thermodynamics integration of the internal energy or pressure avoiding the problems of particle insertion. The advantage of this method is the accuracy with which the energy and pressure can be calculated for these bulk fluid simulations. The disadvantage of this technique is the large number of simulations required to perform accurate calculations of the free energy across the two-phase region. Simulations in the two-phase region often result in large density fluctuation producing metastable fluid structures. The interfacial properties can not be calculated using this technique. These techniques of free energy calculation have been thoroughly reviewed by Frenkel.[6]

Finally phase equilibria can be calculated from a direct simulation of the two coexisting phases using the molecular dynamics method. This method has been applied since 1974 to atomic fluids[13–17] but has not been widely applied to molecular systems. There have been some simulations of diatomic liquids,[18,19] oligomers,[3] methanol,[20] water[1,2,4,21] and water–methanol.[22] In some simulations slab geometries are used with three-dimensional periodic boundary conditions.[2,3,20] Some workers use a system in a rectangular pore with two-dimensional boundary conditions.[15,17,23] The liquid–vapor interface is often close to one of the walls. The advantages of the direct method are the ease of use close to the triple point and the ability to calculate the interfacial properties such as the surface tension and the width of the interface. The disadvantages are thought to be the length of simulation required to stabilize the interface and the difficulty of applying the long-range corrections. The simulation of atomic interfaces has been reviewed by Holcomb.[17]

The purpose of this paper is to perform direct molecular simulations of the liquid–vapor coexistence for water. We plan to address a number of scientific questions.

Can the direct method be used to calculate the orthobaric densities of a strongly dipolar fluid accurately and how do the results of these calculations compare with those obtained

---
[a)]Permanent address: Departamento de Química, Universidad Autónoma Metropolitana-Iztapalapa, Apdo. Postal 55-534, 09340 México D.F, Mexico.

from the Gibbs simulation and thermodynamics integration methods?

Can the temperature dependence of the surface tension be predicted accurately using a pair-additive model for fluid with a large induced dipole in the liquid phase? The effective dipole moment in the simple point charge (SPC/E) model of water[24] is 2.35 D. This dipole moment is modeled by three partial charges at the atomic nuclei and the size of these charges has been adjusted so that the internal energy of the model, including the self-energy term from the induced-dipole accurately fit the experimental measurements. The value of the dipole for the isolated molecule in the gas phase is 1.85 D and there is clearly an effective dipole moment profile through the liquid–vapor interface. There are a number of polarizable models of water that could be used to establish this profile and the effect on the surface tension.[25–27] However, before starting this work on these expensive calculations, we wanted to see if the best effective pair potential for water could reproduce the surface tension at a number of temperatures to within the experimental accuracy. There have been a number of previous simulations to estimate the surface tension of water and these are discussed in Sec. II. The previous results for $\gamma(T)$ are generally poor because of the poor choice of an effective potential for water or the neglect of the long-range part of the dipole–dipole interactions.

Finally, we wished to establish the importance of the long-range part of the dipole–dipole interaction in calculating the surface tension. For fluids such as water there are important long-range corrections to the diagonal elements of the pressure tensor which can be best calculated using an Ewald sum. The convergence of the k-space sum in the direction normal to the interface has been studied and some suggestions are presented for the accurate calculation of $\gamma(T)$.

The paper is organized as follows. Section II contains a discussion of the previous work on the simulation of the liquid–vapor coexistence and surface tension for various models of water. Section III contains a description of the potential model and simulation techniques used in this work. Section IV contains a discussion of the results and Sec. V, our conclusions.

II. PREVIOUS WORK

The first calculations of the coexisting densities and surface tension of water using simulation techniques were developed using small system size and short simulations.[28,29] The results of surface tension are not in good agreement with experiment and definite conclusions cannot be drawn from these studies.

De Pablo et al.[5] have used the SPC and TIP4P for water[30,31] in a Gibbs ensemble calculations. The predicted liquid densities were lower than those observed experimentally and the vapor were higher. The results of the SPC simulations can be reproduced by the direct method and we demonstrate that differences with experiment are due to the use of the SPC model as an effective pair potential.

Guissani and Guillot have performed some highly accurate calculations for the SPC/E model using thermodynamic

integration techniques.[32] They simulated 92 state points using 256 water molecules and constant-NVE molecular dynamics. The long-range interactions were handled using the Ewald sum and the long-range corrections to the energy and pressure from the Lennard-Jones interactions were included in the calculations. The agreement of the orthobaric densities with experiment is good. This work offers a direct comparison with our own and we shall return to this study in the conclusions.

The most extensive calculation of the surface tension and coexisting densities of the liquid–vapor interface for water are reported by Matsumoto and Kataoka.[2] There is a poor agreement between the experimental and simulated surface tensions and coexisting densities. The surface tension, for instance, is less than half of the experimental value. This is most likely to be due to the use of the Carravetta–Clementi ab initio potential, which has not been extensively fitted to experimental liquid-state data.

Wilson et al.[21] calculated the surface tension for the TIP4P model for water at 325 K. The simulated value of the surface tension is 132 mN m^{-1} compared to the experimental value of 68 mN m^{-1}. These authors have indicated that this calculation contains an error[33] and that the correct simulated surface tension for this model[34] at this temperature is 59 mN m^{-1}. The Ewald sum has not been included in either of these simulations. Matsumoto et al.[22] calculated γ for the methanol–water mixtures at 300 K. They used the TIP4P model for water and the TIPS three sites model[35] for methanol. The simulated surface tensions are 20%–50% smaller than those observed experimentally. For pure water they calculated a $\gamma = 50$ mN m^{-1} at 300 K. This value is taken from Fig. 8 of Ref. 22. The long-range corrections to the surface tension of the Lennard-Jones interactions are not included in the calculations of Wilson et al.[21,33] and Matsumoto et al.[22]

Lie et al.[4] have used canonical Monte Carlo methods to simulate the liquid–vapor interface using the MCY model[36] at 298 K. In this work there is no indication of how the long-range interactions are included. The liquid density in the simulation is 0.715 g cm^{-3} and the surface tension is 23.7 mN m^{-1}; the experimental values are 1.0 g cm^{-3} and 72 mN m^{-1}, respectively. The formula for the surface tension appears to be missing a factor of 1/2 in contrast to that used by other workers.[2,3]

In view of the fact that the SPC/E model does such an excellent job for the orthobaric densities and there is considerable uncertainty in the surface tension from a variety of similar models we have performed studies of the liquid–vapor interface of the SPC/E model at six temperatures along the orthobaric curve. In addition we have performed a number of system-size checks for the coexisting densities and surface tensions.

III. INTERACTION MODEL AND SIMULATIONS

We have used the SPC/E model of water throughout this work. The OH bond distances in water are constrained at a separation 1.0 Å. The bond angle interaction is harmonic and is given by

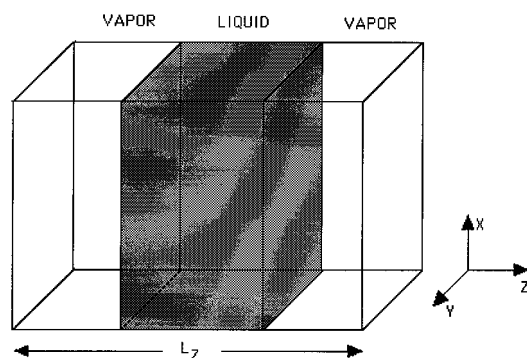$$V = \tfrac{1}{2}k(\theta - \theta_0)^2, \tag{1}$$

FIG. 1. A rectangular parallelepiped cell with a liquid drop in the middle and vapor in each side of the cell. $L_z = 100$ Å for $N = 512$ and 135 Å for $N = 1000$. The z axis is perpendicular to the interface.

where $\theta_0 = 109.47°$ and $k = 383$ kJ mol^{-1} rad^{-2}.

The intermolecular interactions consists of three point charges located at the oxygen and hydrogens sites and include a repulsion-dispersion term modeled by a Lennard-Jones (LJ) potential. The interaction between two water molecules is

$$U(r_{ab}) = 4\epsilon_{OO}\left[\left(\frac{\sigma_{OO}}{r_{OO}}\right)^{12} - \left(\frac{\sigma_{OO}}{r_{OO}}\right)^{6}\right]$$
$$+ \frac{1}{4\pi\epsilon_0}\sum_{a=1}^{3}\sum_{b=1}^{3}\frac{q_a q_b}{r_{ab}}, \tag{2}$$

where q_a is the charge on site a and r_{ab} is the distance between sites a and b on two different molecules. The LJ term is evaluated between the oxygen sites. The LJ parameters are $\sigma_{OO} = 3.166$ Å and $\epsilon_{OO} = 0.6502$ kJ mol^{-1} while $q_O = -0.8476|e|$ and $q_H = -q_O/2$.

The equation of motions are solved using the Verlet algorithm[37] for systems of 512 and 1000 water molecules with a time step of 2.5×10^{-15} s. The constraints are handled using the SHAKE technique.[38] The initial configuration consists of a rectangular parallelepiped with the molecules located in its center, as shown in Fig. 1. The simulation box has a volume $V = L_x L_y L_z$. The sides are of length, $L_x = L_y = 19.7$ Å for $N = 512$ and 23 Å for $N = 1000$. For systems with $N = 512$, $L_z = 100$ Å while $L_z = 135$ Å for $N = 1000$. The molecules are arranged in two replicated cubic boxes along the z direction. Periodic boundary conditions are applied in the three coordinate directions. The electrostatic long range interactions are calculated with the full Ewald summation technique (see Appendix A), with the convergence factor $\kappa = 5.6/L_x$ and the maximum reciprocal lattice vectors parallel to the interface given by $|\mathbf{h}_x^{max}| = |\mathbf{h}_y^{max}| = 5$. As the simulation box is rectangular, $|\mathbf{h}_z^{max}|$ was changed from 10 at 328 K to 20 at 573 K. The increase in $|h_z^{max}|$ makes the simulation significantly longer,[37] but this price must be paid if we want to account for the long-range electrostatic interactions accurately. This is especially important for states near the critical point, where the system becomes more homogeneous and the molecules fill the rectangular cell. The importance of including more reciprocal vectors in

the z-direction is amplified in Appendix B. The short ranged potential cutoff is 9.8 Å, almost half of the smallest side of the box. The systems are equilibrated for 50 000 steps at constant temperature by scaling the velocities at each time-step. The production runs, which are performed at constant energy, consist of 10 blocks for $N = 512$ and 5 blocks for $N = 1000$ of 10 000 steps. In each block, the density profile, the normal and tangential components of the pressure tensor and the surface tension are calculated every 20 steps. The fluctuations in the liquid and vapor densities and surface tension were estimated using the variation in the block averages.

To obtain the surface tension we calculated the components of the pressure tensor using the center of mass definition,[3]

$$\gamma = \frac{1}{2}\langle P_{ZZ} - \frac{1}{2}(P_{XX} + P_{YY})\rangle, \tag{3}$$

where $P_{\alpha\alpha}$ is the $\alpha\alpha$ element of the pressure tensor and $A = L_x L_y$ is the surface area. The factor of 1/2 outside the bracket arises from the two liquid–vapor interfaces in the system. The element $\alpha\beta$ of the molecular pressure tensor is

$$VP_{\alpha\beta} = \sum_{i=1}^{N} m_i(\mathbf{v}_i)_\alpha(\mathbf{v}_i)_\beta$$
$$+ \sum_{i=1}^{N-1}\sum_{j>i}^{N}\sum_{a=1}^{3}\sum_{b=1}^{3}(\mathbf{r}_{ij})_\alpha(\mathbf{f}_{iajb})_\beta, \tag{4}$$

where N is the number of molecules, V is the volume of the system, m_i and $\mathbf{v}_i$ are the molecular mass and velocity of the center of mass, respectively, $\mathbf{r}_{ij}$ is the vector between the center of mass of molecules i and j and

$$\mathbf{f}_{iajb} = -\frac{\mathbf{r}_{iajb}}{r_{iajb}}\left[\frac{dU(r_{iajb})}{dr_{iajb}}\right] \tag{5}$$

is the force between atom a in molecule i and atom b in molecule j. The distance between atom a in molecule i and atom b in molecule j is denoted by r_{iajb}. The definition of the molecular pressure tensor in Eq. (4) is only valid for additive potentials and the calculation of $\mathbf{f}_{iajb}$ and hence $P_{\alpha\beta}$ is in general simple. The constraint forces and the forces arising from bond-angle distortions make no contribution to the molecular pressure tensor.

In the case of the electrostatic interactions treated with the Ewald sum, there are two contributions to the potential, one in the real space (which is pairwise-additive) and other in the reciprocal space (which is not). In the latter case Eq. (4) is not applicable and the appropriate expression is given in Appendix A.

In addition we calculate the normal and tangential component of the pressure tensor as a function of z. For the real space interactions we followed the Irving and Kirwood definition[16] of $\mathbf{P}$ and for the reciprocal space contribution to the potential which is not pairwise additive, we use the Harasima[16] definition of $\mathbf{P}$.

The tangential component of the real space part of the potential in the Irving and Kirwood[16] definition for a planar interface for a molecular system is given by
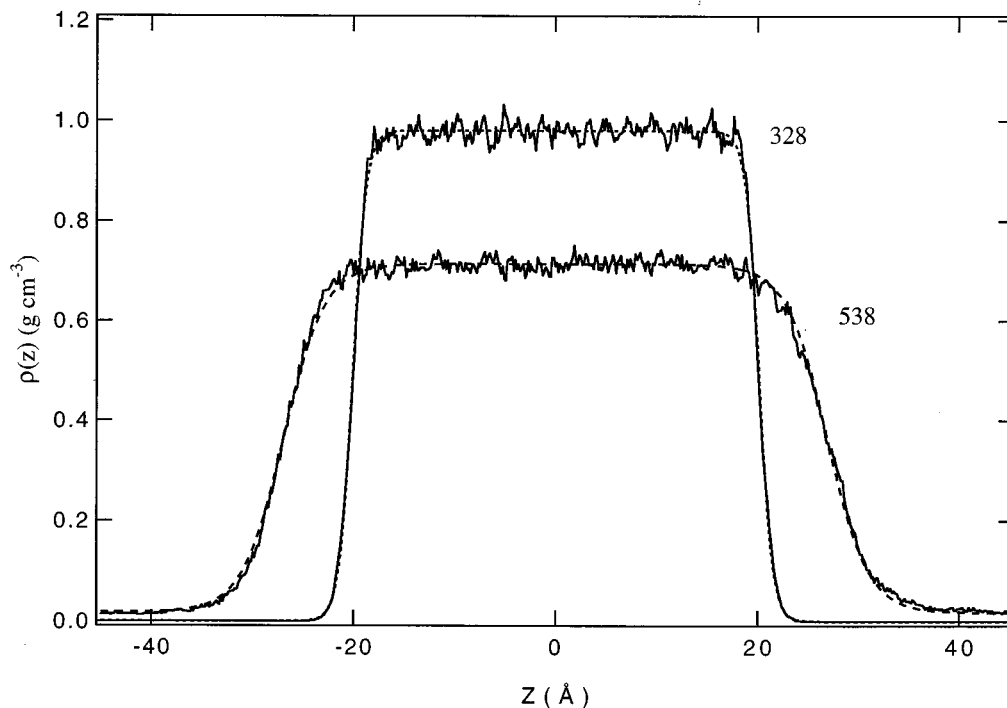
FIG. 2. Density profile as a function of temperature for $N=512$. Continuous line are for MD results and broken line are for the fitted tangent hyperbolic function. The temperature is indicated in each case.

$$P_T(z) = \langle \rho(z) \rangle kT - \frac{1}{A}$$

$$\times \left\langle \sum_{j>i}^{N} \sum_{a}^{3} \sum_{b}^{3} \frac{x_{ij}x_{iajb} + y_{ij}y_{iajb}}{2r_{iajb}} \frac{dU(r_{iajb})}{dr_{iajb}} \frac{1}{|z_{ij}|} \right.$$

$$\left. \times \theta\left(\frac{z-z_i}{z_{ij}}\right) \theta\left(\frac{z_j-z}{z_{ij}}\right) \right\rangle. \tag{6}$$

In this equation $\rho(z)$ is the molecular density profile along the z direction, k is the Boltzmann's constant, T the absolute temperature, $\theta(x)$ is the unit step function [$\theta(x)=0$ when $x<0$ and $\theta(x)=1$ when $x\geq 0$], and U is the real part of the intermolecular potential. The distance z_{ij} is divided into N_s slabs of width Δz and the molecules i and j contribute to the surface tension if the slab contains the line that connects them. Each slab has $1/N_s$ of the total contribution from the $i-j$ interaction. The normal component $P_N(z)$ is given by an expression of the form of Eq. (6) but with $z_{ij}z_{iajb}$ instead of $(x_{ij}x_{iajb}+y_{ij}y_{iajb})/2$. Equations (4) and (6) correct Eq. (4.5) of Thompson[18] for the surface tension.

The normal and tangential components of the reciprocal space part of the pressure tensor have two contributions, see Eq. (A10). These contributions are calculated as follows: To calculate the second term as a function of z in Eq. (A10), the contribution to the surface tension of each molecule is the same for all molecules and is given by the component divided by the number of molecules. The second contribution of the reciprocal space part was calculated using Eq. (A11).

In this case the surface tension contribution is attributed to the z-slab containing the center of mass of a particular molecule.

The surface tension can be calculated from the components of the pressure tensor using

$$\gamma = \frac{1}{2} \int_{-\infty}^{\infty} [P_N(z) - P_T(z)] dz. \tag{7}$$

The surface tension calculated with Eqs. (3) and (7) must be the same. The advantage of calculating the components as a function of z is that we can establish that the system is at equilibrium by checking that $P_N(z)$ is constant and $P_N(z)=P_T(z)$ away from the interfaces.

IV. RESULTS AND DISCUSSIONS

Once the system has reached the equilibrium and the interface has been formed, the properties are calculated. Runs of 10^5 time steps are required to calculate the surface tension accurately. The orthobaric densities can be accurately estimated with half this number of time steps.

Typical density profile at two different temperatures are shown in Fig. 2. A hyperbolic tangent function of the form[15]

$$\rho(z) = \tfrac{1}{2}(\rho_L + \rho_V) - \tfrac{1}{2}(\rho_L - \rho_V)\tanh[(z-z_0)/d] \tag{8}$$

is fitted to the simulation results. In Eq. (8) ρ_L and ρ_V are the densities of the liquid and the vapor in the bulk phases, z_0 is the position of the Gibbs' dividing surface, and d is a parameter for thickness of the interface. The fitted $\rho(z)$ are shown

TABLE I. The molecular temperature, orthobaric densities, and the 10–90 thickness of the interface for systems with 512 and 1000 molecules. γ_R and γ_K are the real and reciprocal space contributions to the surface tension. γ_{tail} is the tail correction for the truncated repulsion-dispersion interaction. The total surface tension γ is given with the estimated error in brackets.

| | | | | | γ/mN m^{-1} | | | |
N	T/K	ρ_L/g cm^{-3}	ρ_V/g cm^{-3}	thickness/Å	γ_R	γ_K	γ_{tail}	γ_{total}
512	328	0.981	0.0001	2.99	46.8	13.7	5.5	66.0(3.0)
512	367	0.944	0.0003	3.62	44.3	9.2	5.0	58.5(3.2)
512	435	0.875	0.0006	5.33	31.6	10.0	4.1	45.7(3.4)
512	479	0.815	0.0052	6.60	24.7	11.3	3.3	39.3(3.5)
512	538	0.714	0.0176	8.93	10.6	7.3	2.2	20.1(3.5)
512	573	0.610	0.0583	10.42	8.4	7.8	1.5	17.7(4.0)
1000	316	0.984	0.0001	3.13	59.7	7.7	4.1	71.5(3.5)
1000	411	0.903	0.0003	5.05	39.5	10.4	3.3	53.2(3.7)
1000	504	0.775	0.0124	8.12	18.8	10.1	1.9	30.8(4.1)

as dashed lines in Fig. 2. The liquid and vapor equilibrium densities and the parameters used in Eq. (8) are given in Table I for all the states points studied.

It is clear from the profiles that a well defined interface is established and there is a region of bulk liquid of approximately 36 Å thickness between the two surfaces. The liquid region is wide enough to make an accurate estimate of the liquid density and the profile is symmetric around the middle of the slab.

For the hyperbolic tangent function the "10–90 thickness," t, is related to d by $t = 2.1972 d$. The thickness, t, can be obtained indirectly from ellipsometric and x-ray reflectivity experiments. Matsumoto[2] has reported that for water at 300 K the 10–90 thickness obtained from ellipsometric and x-ray reflectivity experiments is 4.1 and 8.3 Å, respectively. Schwartz et al.[40] measured the surface roughness, $\langle s^2 \rangle$, of water at 298 K using x-ray reflectivity experiments and obtained a value of 2.8 Å. For a hyperbolic tangent function the 10–90 thickness is equal[41] to $2.423\langle s^2 \rangle$ or 6.91 Å. There are large differences between the experimental values and it is hard to make definitive conclusions when comparing them with the results obtained in the simulations. Figure 3 shows t as a function of temperature from simulation and experiment. The 10–90 thickness obtained in our simulations is also given in Table I. The values obtained for the SPC/E model of water from the simulation are almost independent of system size but they lie well below the values obtained for the CC (Ref. 2) and MCY (Ref. 4) models. One reason for this is that MCY and CC models predict low liquid densities and high vapor compared with experiment and with the SPC/E model. This results in the high value of t for the MCY and CC model.

Although there is considerable scatter in the experimental results it is clear that the agreement with the CC and MCY model is better than with the SPC/E model. We believe that the SPC/E model gives a more accurate account of the intrinsic interfacial width and that the experimental estimates are increased by the capillary waves, which are absent in the simulation. We suggest that the good agreement with the MCY and CC models is fortuitous.

In Fig. 4(a) we present the MD results of the liquid and vapor densities for SPC/E water and its comparison with the SPC model calculated by de Pablo et al.[5] using the GEMC method. The agreement with experimental densities[42] is better for the SPC/E model than for the SPC model. We can easily demonstrate that the difference between the SPC and SPC/E densities is a consequence of the different models and not the different simulation techniques employed in the studies. We have performed one MD simulation of the SPC model at 475 K. This result is shown as a solid square in Fig. 4(a), the result is in good agreement with the results of de Pablo et al.[5] for the same model at the same temperature. Although the SPC/E model is an improvement over the SPC model the agreement with experiment becomes poorer at higher temperatures. The truncation of the repulsion-dispersion interactions is known to affect the liquid–vapor densities of the Lennard-Jones fluid in simulations using the direct method.[15–17] We cannot see an easy way to correct for this truncation in the density profile themselves, although it is straightforward to correct the resulting surface tension. To explore this problem in more detail we have performed some
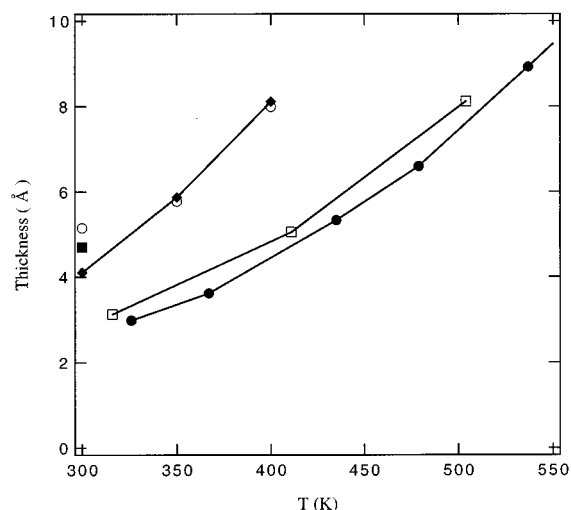
FIG. 3. The 10–90 thickness of the interface as a function of temperature. Black diamond are the experimental values taken from Ref. 2. Black circles are from this work with $N=512$. Open squares are from this work with $N=1000$. The single black square is for the MCY potential (Ref. 4) and the open circles are for CC potential (Ref. 2). The lines through the values are given to help the eye.
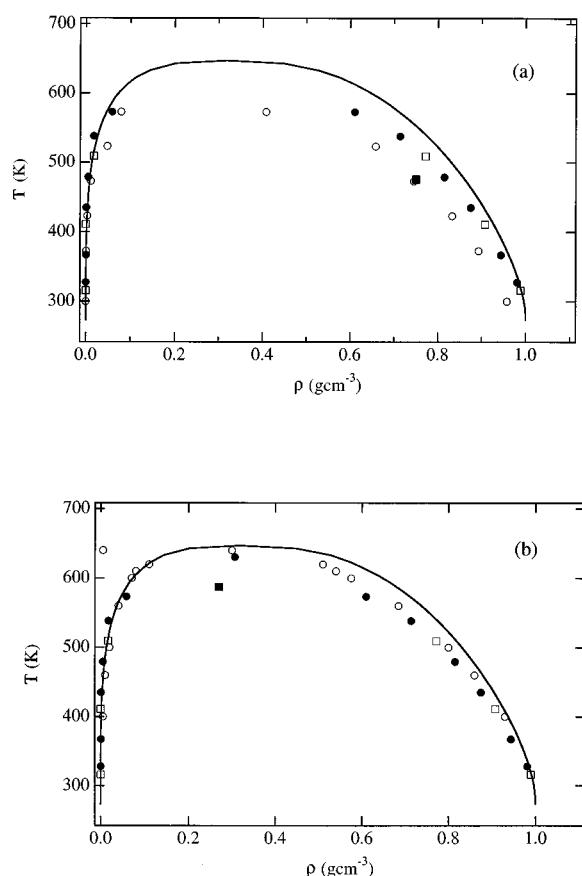
FIG. 4. The orthobaric densities for water. The continuous line represents the experimental values (Ref. 42). Black circles are for this work using $N=512$. Open squares are for this work using $N=1000$. (a) Open circles are GEMC results (Ref. 5) using the SPC potential. The black squares are our MD results using the SPC model and $N=512$. (b) Open circles are results from Ref. 32. The black square is the critical point of the SPC model calculated using the GEMC technique (Ref. 5).

simulations using 1000 molecules at a cutoff of 11.5 Å ($3.63\sigma_{OO}$). The results are shown as open squares in Fig. 4(a). We can see very little change in the coexisting densities with system size or cutoff and it appears that the long-range corrections associated with the charges and handled using the Ewald method are much more important that the correction due to the repulsion-dispersion interactions. A comparison between our liquid–vapor densities and those calculated by Guissani and Guillot[32] for the SPC/E water model using the thermodynamic integration method of free energies, is shown in Fig. 4(b). The coexisting densities were obtained from Figs. 3 and 4 of Ref. 32. Good agreement is obtained across the whole temperature range studied.

We estimated the critical point for the SPC/E model by fitting the liquid–vapor data to the law of rectilinear diameters and the appropriate scaling law for the density using a scaling exponent of 0.33. The critical temperature and density calculated from this analysis are 630.4 K and 0.308 g cm^{-3}, respectively. This in contrasts with the values obtained by Guissani and Guillot, 640 K and 0.29 g cm^{-3}, using the power law expansions Eqs. (5) and (6) in their paper.

A. Normal and tangential components

In Fig. 5(a), we present the difference between the normal and tangential components of the pressure tensor for the real space pair additive potentials at 328 K as a function of z. In the bulk phases the normal and tangential pressure must be equal, i.e., the difference should be zero. The tangential pressure must exhibit a negative region at the interface. These two features are shown in Fig. 5(a), where the symmetric peaks are due to $P_T(z)$. The $P_N(z)$ is, as expected, constant through the interface.

The surface tension can be measured at as a function of z by integrating $P_N(z)-P_T(z)$. Its value must be constant in the bulk phases and increase at the interfaces. $\gamma(z)$ is shown at 328 K in Fig. 5(b). The system is well equilibrated and the contribution from both surfaces is the same. Figures 5(c) and 5(d) show the corresponding results for the pressure tensor arising from the long-range electrostatic interactions.

B. Surface tension

We have calculated the surface tension during the simulation using Eq. (3) and integrating the difference between the normal and tangential components after the simulation with Eq. (7). In both cases the value is the same within the estimated error in the simulation. For the Lennard-Jones potential the surface tension is essentially independent of the cutoff radius if the long range corrections are applied.[17] In our case, oxygens in water interact through a repulsion-dispersion potential and an electrostatic potential and the appropriate long-range corrections are applied using a molecular field theory with $g(s_{12},z_1,z_2)=1$. The electrostatic interactions are handled using the Ewald method. Since the simulation cell is rectangular, the number of lattice vectors (used in the reciprocal space part of the Ewald sum) in the z direction must be greater than those in x and y directions. We found that using the same small number of lattice vectors in the three directions overestimates the surface tension. The contributions to the surface tension are given in Table I. Figure 7 shows the behavior of γ as a function of $|\mathbf{h}_z^{max}|$. Clearly at $T=538$ K truncating the reciprocal lattice sum at $|\mathbf{h}_z^{max}| = 5$ would significantly overestimate the surface tension. Table II shows the effect of changing $|\mathbf{h}_z^{max}|$ on the instantaneous surface tension at 328 and 538 K for a given configuration of liquid–vapor interface of water. At 538 K γ_K^I and γ_K^{II} [which derive from the second and third term in Eq. (A10)] change sign when $|\mathbf{h}_z^{max}|$ changes from 15 to 20. The contribution of the reciprocal space to the surface tension varies with temperature, being 15% at 328 K and 42% at 573 K.

The tail correction to the surface tension for the LJ interactions is evaluated following Chapela et al.,[15]

$$\gamma^{tail} = 12\pi\epsilon \int_{-\infty}^{\infty} \int_{-1}^{1} \int_{r_c}^{\infty} \rho(z_1)\rho(z_2)$$

$$\times (1-3s^2)r^{-4} \, dr \, ds \, dz_1, \tag{9}$$

where $s=(z_1-z_2)/r$ and z_1 and z_2 are the positions of molecules 1 and 2. As $\rho(z)$ is represented by a hyperbolic tangent function [Eq. (8)], Eq. (9) is integrated over z_1 to give
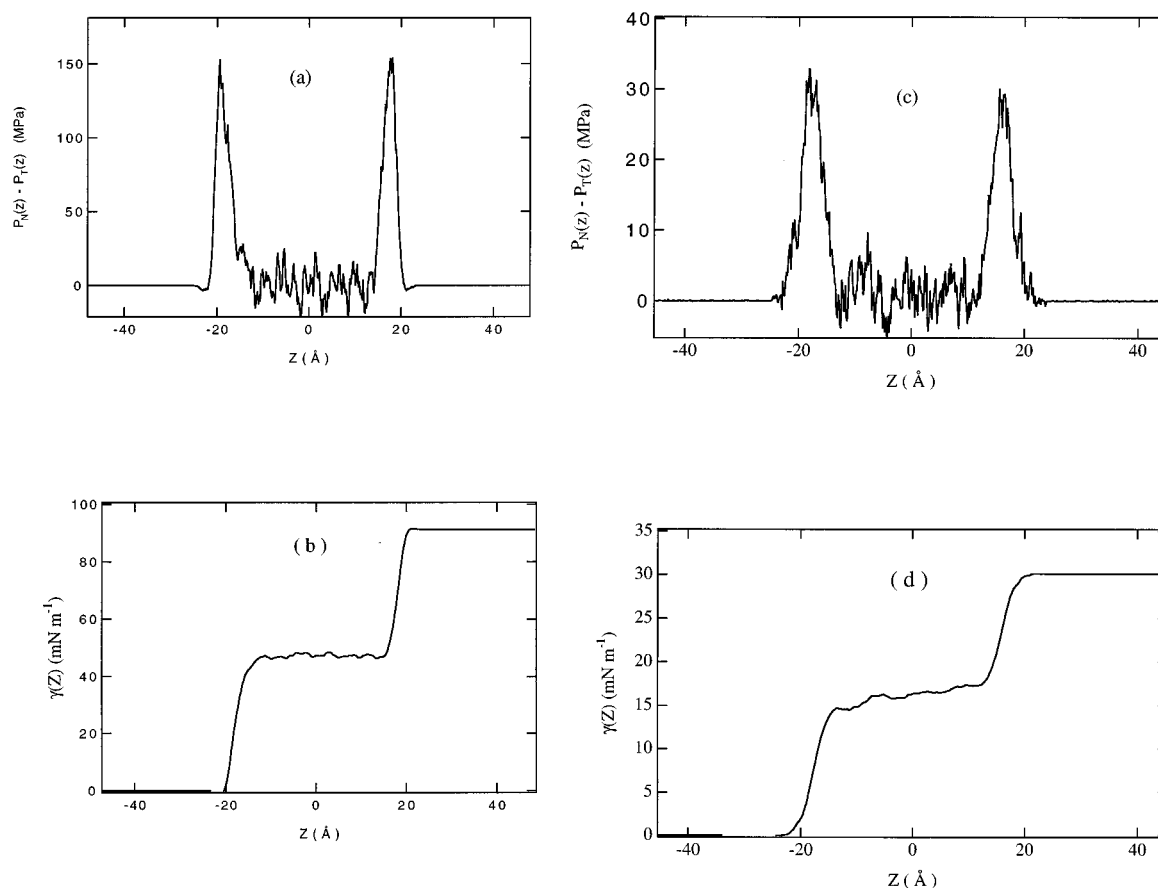
FIG. 5. (a) $P_N(z)-P_T(z)$ for the real part of the potential as a function of z at 328 K and $N=512$. (b) The integral of $P_N(z)-P_T(z)$ from the real part of the potential as a function of z at 328 K and $N=512$. (c) $P_N(z)-P_T(z)$ from the reciprocal space part of the potential as a function of z at 328 K and $N=512$. (d) The integral of $P_N(z)-P_T(z)$ of the reciprocal space part of the potential as a function of z at 328 K and $N=512$.

$$\gamma_{tail}=12\pi\epsilon\sigma^6(\rho_L-\rho_V)^2\int_0^{+1}ds\int_{r_c}^{+\infty}dr\ \coth(rs/d)$$

$$\times(3s^3-s)r^{-3} \qquad (10)$$

where r_c is the cutoff radius. This result recently derived by Blokhuis et al.[48] corrects equation (A5) of Ref. 15. The tail correction to the surface tension decreases as temperature increases.

As shown in Fig. 6, the surface tension decreases as temperature increases and excellent agreement with experiment is obtained for the SPC/E model.

V. CONCLUSIONS

The results in this paper indicate that the direct simulation method of studying two phases in coexistence is a useful way for predicting the liquid–vapor equilibria. The method can be readily used at the triple point, since it does not suffer from the problem with particle insertions which limit the Gibbs ensemble Monte Carlo method. By performing one simulation of the SPC model, we were able to demonstrate the Gibbs and direct simulation methods give consistent results for the same effective potential. The results for the coexisting densities are also consistent with those calculated using thermodynamic integration of the free energy obtained from 92 bulk simulations. The agreement is good for all the temperatures studied in this work. In summary, we have shown that for the same potential the direct MD method reproduce, within the error in the simulation, the coexisting densities calculated using the GEMC method or the thermodynamics integration route.

The results of this study show that the SPC/E model of water gives better account of the orthobaric densities and surface tensions that either the SPC or TIP4P models. There are still some differences between the simulated and experimental densities at high temperatures but that can be understood since the SPC/E potential was fitted to reproduce experimental results of water at 300 K.

An important conclusion of this work is that the SPC/E effective pair potential can accurately reproduce the experimental surface tension of water over the temperature range 300–600 K. The simulated surface tension at all but the highest temperatures are within one standard deviation of the experimental measurements. It is not essential to employ a polarizable model of water, or allow for an effective dipole moment profile to model the surface tension accurately.

The long-range dipole–dipole interactions between the water molecules make an important contribution to the surface tension. We have demonstrated the importance of using an Ewald sum in the calculation of $\gamma(T)$. For instance, for a simulation performed in the two-phase region using 512 water molecules, close to the experimental triple point, the re-
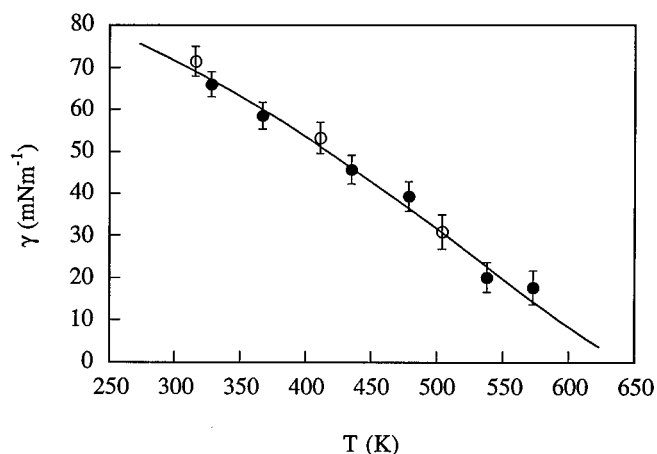
FIG. 6. The surface tension of water. The continuous line represents experimental values (Ref. 42). MD results using $N=512$ and $N=1000$ are shown with black and open circles, respectively.

ciprocal space contribution to γ is 20% at 328 K rising to 42% at 573 K. The corresponding corrections from the long-range part of the dispersion interaction are 8.3% and 8.5%, respectively. It is important to remember that because of the long-range interactions the two interfaces cannot be completely independent.

The simulations are performed in a rectangular parallelepiped that is elongated in the z-direction. This means that the sum over the reciprocal lattice vectors in the z-direction must be increased to include shorter wavelength vectors. In this study, we used $|\mathbf{h}_x^{max}| = |\mathbf{h}_y^{max}| = 5$ and $|\mathbf{h}_z^{max}| = 20$ for points close to the critical point for systems of 512 molecules. Failure to extend the range of the z-sum can result in a reciprocal space contribution with the wrong sign. The results are unaffected by increasing $|\mathbf{h}_x^{max}|$ and $|\mathbf{h}_y^{max}|$ beyond 5. A check using 500 and 1000 molecules indicates that γ is essentially unchanged on increasing the system size in the simulation.
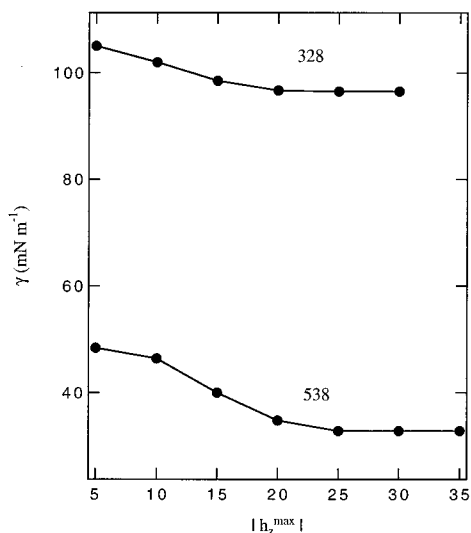

FIG. 7. The instantaneous surface tension, γ, as a function of $|\mathbf{h}_z^{max}|$ at 328 K and 538 K with $N=512$.

APPENDIX A: ENERGY, FORCES, AND PRESSURE TENSOR FOR ELECTROSTATIC INTERACTIONS IN THE EWALD METHOD

The equations given here were derived by following the same procedure as Nosé and Klein.[43,44] We give them for completeness, to make the comparison with other studies and to point out some misprints.

Consider N molecules in a volume $V=L_xL_yL_z$ with center of mass $\mathbf{r}_i$, each molecule contains n_i charges q_{ia} at position $\mathbf{r}_{ia}$. The potential energy in the Ewald sum for a box with orthogonal axis is written as[43–45]

$$U=\frac{2\pi}{V}\sum_{\mathbf{h}\neq 0} Q(h)S(\mathbf{h})S(-\mathbf{h})$$
$$+\frac{1}{2}\sum_i\sum_a\sum_{j\neq i} q_{ia}\sum_b q_{jb}\,\mathrm{erfc}(\kappa r_{iajb})/r_{iajb}$$
$$-\frac{\kappa}{\sqrt{\pi}}\sum_i\sum_a q_{ia}^2$$
$$-\frac{1}{2}\sum_i\sum_a\sum_{b\neq a} q_{ia}q_{ib}\,\mathrm{erf}(\kappa r_{iaib})/r_{iaib}, \qquad (A1)$$

where $\mathrm{erfc}(x)$ is the complementary error function, $\mathrm{erf}(x)$ is the error function, κ is an arbitrary convergence parameter which damps the real space interaction and is chosen so that only pair interactions in the central cell need to be considered in evaluating the second term in Eq. (A1), and

TABLE II. The effect of changing $|h_z^{max}|$ on γ at two temperatures for systems with $N=512$. γ_K^I and γ_K^{II} arise from the second and third term in the pressure tensor, Eq. (A10). γ_K^{II} was calculated using Eq. (A11). The units of γ are mN m^{-1}. The Ewald convergence factor is $\kappa=5.6/L_x$.

$|h_z^{max}|$	γ_R	γ_K^I	γ_K^{II}	γ
$T=328$ K				
5	94.5	9.5	1.0	105.0
10	94.5	6.5	1.0	102.0
15	94.5	1.5	2.5	98.5
20	94.5	−0.3	2.5	96.7
25	94.5	−0.5	2.5	96.5
30	94.5	−0.5	2.5	96.5
$T=538$ K				
5	37.2	15.6	−4.4	48.4
10	37.2	15.2	−6.0	46.4
15	37.2	2.8	0.0	40.0
20	37.2	−4.8	2.4	34.8
25	37.2	−7.2	2.8	32.8
30	37.2	−7.6	2.8	32.8
35	37.2	−7.6	2.8	32.8

$$S(\mathbf{h}) = \sum_i \sum_a q_{ia} \exp(i\mathbf{h}.\mathbf{r}_{ia}), \tag{A2}$$

$$Q(h) = \exp(-h^2/4\kappa^2)/h^2, \tag{A3}$$

$$\mathbf{r}_{iajb} = \mathbf{r}_{ia} - \mathbf{r}_{jb}, \tag{A4}$$

where the reciprocal lattice vector $\mathbf{h}$ is defined as

$$\mathbf{h} = 2\pi(l/L_x, m/L_y, n/L_z), \tag{A5}$$

where l, m, and n take values $0, \pm1, \pm2, ...\pm\infty$.

In a simulation the condition $|\mathbf{h}|^2 \leqslant |\mathbf{h}_{max}|^2$ is applied, the choice of $|\mathbf{h}_{max}|$ is dependent on the convergence parameter κ. The contribution of the reciprocal space part of the potential becomes more important with increasing κ.

The force on atom a of molecule i is given by

$$\mathbf{F}_{ia} = -\frac{\partial U}{\partial \mathbf{r}_{ia}} = \mathbf{F}_{ia}^R + \mathbf{F}_{ia}^K, \tag{A6}$$

where $\mathbf{F}_{ia}^R$ is the force acting on atom a of molecule i coming from the real space and $\mathbf{F}_{ia}^K$ that of the reciprocal space,

$$\mathbf{F}_{ia}^R = \frac{q_{ia}}{4\pi\epsilon_0} \sum_{j\neq i} \sum_b q_{jb}\left[\frac{2}{\sqrt{\pi}}\kappa r_{iajb}\exp(-\kappa^2 r_{iajb}^2)\right.$$

$$\left. + \mathrm{erfc}(\kappa r_{iajb})\right]\frac{\mathbf{r}_{iajb}}{r_{iajb}^3}, \tag{A7}$$

$$\mathbf{F}_{ia}^K = \frac{q_{ia}}{4\pi\epsilon_0}\left\{\frac{2\pi}{V}\sum_{\mathbf{h}\neq 0}Q(h)i\mathbf{h}[S(\mathbf{h})\exp(-i\mathbf{h}.\mathbf{r}_{ia})\right.$$

$$\left. - S(-\mathbf{h})\exp(i\mathbf{h}.\mathbf{r}_{ia})]\right\}, \tag{A8}$$

or in a more convenient notation for a simulation

$$\mathbf{F}_{ia}^K = -\frac{q_{ia}}{4\pi\epsilon_0}\left\{\frac{4\pi}{V}\sum_{\mathbf{h}\neq 0}Q(h)\mathbf{h}\right.$$

$$\left. \times \mathrm{Imag}[\exp(-i\mathbf{h}.\mathbf{r}_{ia})S(\mathbf{h})]\right\}, \tag{A9}$$

where Imag denotes the imaging part of the complex variable.

The pressure tensor is

$$VP_{\alpha\beta} = \frac{1}{8\pi\epsilon_0}\sum_i \sum_a q_{ia}\sum_{j\neq i}\sum_b q_{jb}\left[\frac{2}{\sqrt{\pi}}\kappa r_{iajb}\exp(-\kappa^2 r_{iajb}^2) + \mathrm{erfc}(\kappa r_{iajb})\right]\frac{(\mathbf{r}_{ij})_\alpha (\mathbf{r}_{iajb})_\beta}{r_{iajb}^3}$$

$$+ \frac{1}{4\pi\epsilon_0}\left[\frac{2\pi}{V}\sum_{\mathbf{h}\neq 0}Q(h)S(\mathbf{h})S(-\mathbf{h})\left(\delta_{\alpha\beta} - \frac{2\mathbf{h}_\alpha\mathbf{h}_\beta}{h^2} - \frac{\mathbf{h}_\alpha\mathbf{h}_\beta}{2\kappa^2}\right)\right]$$

$$- \frac{1}{4\pi\epsilon_0}\left\{\frac{2\pi}{V}\sum_i \sum_a (\mathbf{p}_{ia})_\beta q_{ia}\sum_{\mathbf{h}\neq 0}Q(h)i\mathbf{h}_\alpha[S(\mathbf{h})\exp(-i\mathbf{h}.\mathbf{r}_{ia}) - S(-\mathbf{h})\exp(i\mathbf{h}.\mathbf{r}_{ia})]\right\} \tag{A10}$$

with $\delta\alpha\beta$ the Kronecker delta, $\mathbf{p}_{ia} = \mathbf{r}_{ia} - \mathbf{r}_i$ is a vector between atom a in the molecule i and the center of mass of molecule i. This result for the pressure tensor was originally derived by Nosé and Klein.[43] However Eq. (A10) of this work *differs* from Eq. (A8) of Ref. 40 where the factor q_{ia} is missed from the last term.

These results have been independently derived by Heyes.[46] The connection with his formulation can be made by using Eq. (A8) to manipulate the last term in Eq. (A10) to give

$$-\left[\sum_i \sum_a (\mathbf{r}_{ia} - \mathbf{r}_i)_\beta(\mathbf{F}_{ia}^K)_\alpha\right]. \tag{A11}$$

This equation *differs* from Eq. (21) of Heyes.[46] In this case the vector in brackets is between atom a in molecule i and the center of mass of molecule i while in Heyes[46] it is simply the position of atom a in molecule i. Equation (A11) is correct.[47] We have checked that both these formulations are consistent.

APPENDIX B: RECIPROCAL LATTICE VECTORS IN RECTANGULAR BOXES

In simulations of the liquid–vapor interface the simulation box is normally a rectangular parallelepiped with the liquid as a slab in the middle of a periodically repeating box. For systems with electrostatic interactions handled using the Ewald technique, care has been taken in choosing the reciprocal lattice vectors $\mathbf{h}$. The density of the lattice vectors must be constant in changing from cubic box to a rectangular parallelepiped. The number of vectors has to be increased in the z direction.

We can illustrate this point using a simple example. Suppose that we have N molecules with n_i atoms, at position $\mathbf{r}_{ia}$ with charge q_{ia} in a cubic box and that the electrostatic interactions are calculated using the Ewald method. The energy of the system is U. If the system is duplicated along z, $L_z = 2L_z$, the energy for the new system, $2U$, is given by Eq. (A1) with N replaced by $2N$, $V = L_xL_y(2L_z)$ and $\mathbf{r}_{i+N} = \mathbf{r}_i + (0,0,L_z)$. To evaluate the reciprocal sum we must use a new set of reciprocal lattice vectors given by

$$\mathbf{h}^r = 2\pi(l/L_x, \ m/L_y, \ n^r/2L_z), \tag{B1}$$

where $l = 0, \pm 1, \ldots, \pm l_{max}$, $m = 0, \pm 1, \ldots, \pm m_{max}$, and $n^r = 0, \pm 1, \ldots, \pm n^r_{max}$. $S^r(\mathbf{h})$ for the replicated system (superscript r) can be written in terms of $S(\mathbf{h})$ for the original system as

$$S^r(\mathbf{h}) = S(\mathbf{h}) + S(\mathbf{h}) \sum_{j=N+1}^{2N} \sum_{a=1}^{n_j} q_{ja} e^{i\mathbf{h}.(0,0,L_z)} \tag{B2}$$

or

$$S^r(\mathbf{h}) = S(\mathbf{h}) + S(\mathbf{h})(-1)^{n^r}. \tag{B3}$$

$S^r(\mathbf{h}) = 0$ for n^r odd and $S^r(\mathbf{h}) = 2S(\mathbf{h})$ for n^r even. In this particular case, where the size of the basic cell is doubled in one direction and the particle positions replicated, the odd elements do not contribute. Substituting Eq. (B3) in Eq. (A1) we can show that $U^r = 2U$, but it is necessary to take $n^r_{max} = 2l_{max} = 2m_{max}$. In other words, the range of the z sum has to be doubled.

The box used in our simulations of $N = 512$ is approximately in the ratio 1:1:5 and to achieve convergence we find that $|\mathbf{h}_z^{max}|$ has to be increased to 20 at temperatures greater than 500. Note that in our system none of the terms in the $\mathbf{h}_z$ sum is identically zero.

[1] A. R. van Buuren, S-J. Marrink, and H. J. C. Berendsen, J. Phys. Chem. **97**, 9206 (1993).

[2] M. Matsumoto and Y. Kataoka, J. Chem. Phys. **88**, 3233 (1988).

[3] J. G. Harris, J. Phys. Chem. **96**, 5077 (1992).

[4] G. C. Lie, S. Grigoras, L. X. Dang, D-J. Yang, and D. Mclean, J. Chem. Phys. **99**, 3933 (1993).

[5] (a) J. J. de Pablo, J. M. Prausnitz, H. J. Strauch, and P. T. Cummings, J. Chem. Phys. **93**, 7355 (1990); (b) J. J. de Pablo and J. M. Prausnitz, Fluid Phase Equilib. **53**, 177 (1989).

[6] D. Frenkel, in *Computer Simulation in Chemical Physics*, edited by M. P Allen and D. J. Tildesley (Kjeuver, New York, 1993), pp. 93–152.

[7] B. Smit, in *Computer Simulation in Chemical Physics*, edited by M. P. Allen and D. J. Tildesley (Kjeuver, New York, 1993), pp. 173–210.

[8] A. Z. Panagiotopoulos, Mol. Phys. **61**, 813 (1987).

[9] A. Z. Panagiotopoulos, N. Quirke, M. R. Stapleton, and D. J. Tildesley, Mol. Phys. **63**, 527 (1988).

[10] J. J. de Pablo, M. Laso, J. I. Siepmann, and U. W. Suter, Mol. Phys. **80**, 55 (1993).

[11] J. I. Siepmann, S. Karaborni, and B. Smit, Nature **365**, 330 (1993).

[12] M. R Stapleton and A. Z. Panagiotopoulos, J. Chem. Phys. **92**, 1285 (1990).

[13] J. K. Lee, J. A. Barker, and G. M. Pound, J. Chem. Phys. **60**, 1976 (1974).

[14] G. A. Chapela, G. Saville, and J. S. Rowlinson, Faraday Discuss. Chem. Soc. **59**, 22 (1975).

[15] G. A. Chapela, G. Saville, S. M. Thompson, and J. S. Rowlinson, J. Chem. Soc. Faraday Trans. II **8**, 133 (1977).

[16] J. P. R. B. Walton, D. J. Tildesley, and J. S. Rowlinson, Mol. Phys. **48**, 1357 (1983).

[17] D. C. Holcomb, P. Clancy, and J. A. Zollweg, Mol. Phys. **78**, 437 (1993).

[18] S. M. Thompson, Faraday Discuss. Chem. Soc. **66**, 107 (1978).

[19] C. A. Croxton, *Statistical Mechanics of the Liquid Surface* (Wiley, New York, 1980).

[20] M. Matsumoto and Y. Kataoka, J. Chem. Phys. **90**, 2398 (1989).

[21] M. A. Wilson, A. Pohorille, and L. R. Pratt, J. Phys. Chem. **91**, 4873 (1987).

[22] M. Matsumoto, Y. Takaoka, and Y. Kataoka, J. Chem. Phys. **98**, 1464 (1993).

[23] G. A. Chapela, S. E. Martínez-Casas, and C. Varea, J. Chem. Phys. **86**, 5683 (1987).

[24] H. J. C. Berendsen, J. R. Grigera, and T. P. Straatsma, J. Phys. Chem. **91**, 6269 (1987).

[25] M. Sprik, J. Phys. Chem. **95**, 2283 (1991).

[26] M. Sprik and M. L. Klein, J. Chem. Phys. **89**, 7556 (1988).

[27] L. Dang, J. Chem. Phys. **97**, 2659 (1992).

[28] B. Bornstnik, D. Janezic, and A. Azman, Acta Phys. Acad. Sci. Hung. **48**, 297 (1980).

[29] C. Y. Lee and H. L. Scott, J. Chem. Phys. **73**, 4591 (1980).

[30] H. J. C. Berendsen, J. P. M. Postma, W. F. van Gunsteren, and H. J. Hermans, in *Intermolecular Forces*, edited by Pullman (Reidel, Dordrecht, 1981).

[31] W. L. Jorgensen, J. Chandrasekhar, J. D. Madura, R. W. Impey, and M. L. Klein, J. Chem. Phys. **79**, 926 (1983).

[32] Y. Guissani and B. Guillot, J. Chem. Phys. **98**, 8221 (1993).

[33] L. R. Pratt, A. Pohorille, and M. A. Wilson (personal communication, 1994).

[34] (a) L. R. Pratt and A. Pohorille, *Water–Biomolecule Interactions*, edited by M. U. Palma, M. B. Palma-Vittorelli, and F. Parak (SIF, Bologna, 1993), Vol. 43; (b) A. Pohorille and M. A. Wilson, J. Mol. Struct. (TheoChem) **284**, 271 (1993).

[35] W. L. Jorgensen, J. Am. Chem. Soc. **103**, 335 (1981).

[36] O. Matsouka, E. Clementi, and M. Yoshimine, J. Chem. Phys. **64**, 1351 (1976).

[37] M. P. Allen and D. J. Tildesley, *Computer Simulations of Liquids* (Clarendon, Oxford, 1987).

[38] J-P. Ryckaert, G. Ciccoti, and H. J. C. Berendsen, J. Comp. Phys. **23**, 327 (1977).

[39] The experimental values of the thickness of the interface of water were taken from Ref. 2 of this paper.

[40] D. K. Schwartz, E. K. Schlossman, G. J. Kellogg, P. S. Pershan, and B. M. Ocko, Phys. Rev. A **41**, 5687 (1990).

[41] E. A. Simister, E. M. Lee, R. K. Thomas, and J. Penfold, J. Phys. Chem. **96**, 1373 (1992).

[42] *International Critical Tables* (McGraw–Hill, New York, 1928), Vol. III.

[43] S. Nosé and M. L. Klein, Mol. Phys. **50**, 1055 (1983).

[44] S. Nosé and M. L. Klein, in *Simulation of Liquids and Solids*, edited by G. Ciccotti, D. Frenkel, and I. R McDonald (North–Holland, Amsterdam, 1987).

[45] S. W. de Leeuw, J. W. Perram, and E. R. Smith, Proc. R. Soc. London, Ser. A **373**, 27 (1980).

[46] D. M. Heyes, Phys. Rev. B **49**, 755 (1994).

[47] D. M. Heyes (personal communication, 1994).

[48] E. M. Blokhuis, D. Bedeaux, C. D. Holcomb, and J. A. Zollweg, submitted to Mol. Phys.